Gravitational waves from very massive stars collapsing to a black hole

Haruki Uchida,[1] Masaru Shibata,[2,1] Koh Takahashi,[3] and Takashi Yoshida[4]

[1]*Yukawa Institute for Theoretical Physics, Kyoto University, Kyoto 606-8502, Japan*
[2]*Max Planck Institute for Gravitational Physics (Albert Einstein Institute),*
Am Muhlenberg 1, Potsdam-Golm 14476, Germany
[3]*Argelander-Institut für Astronomie, Universiät Bonn, D-53121 Bonn, Germany*
[4]*Department of Astronomy, Graduate School of Science, the University of Tokyo, Tokyo 113-0033, Japan*

We compute gravitational waves emitted by the collapse of a rotating very massive star (VMS) core leading directly to a black hole in axisymmetric numerical-relativity simulations. The evolved rotating VMS is derived by a stellar evolution calculation, and its initial mass and the final carbon-oxygen core mass are 320 $M_\odot$ and $\approx$150 $M_\odot$, respectively. We find that, for the moderately rapidly rotating cases, the peak strain amplitude and the corresponding frequency of gravitational waves are $\sim 10^{-22}$ and $f \approx$ 300–600 Hz for an event at the distance of $D = 50$ Mpc. Such gravitational waves will be detectable only for $D \lesssim$ 10 Mpc by second-generation detectors, advanced LIGO, advanced VIRGO, and KAGRA, even if the designed sensitivity for these detectors is achieved. However, third-generation detectors will be able to detect such gravitational waves for an event up to $D \sim 100$ Mpc. The detection of the gravitational-wave signal will provide a potential opportunity for verifying the presence of VMSs with mass $\gtrsim$300 $M_\odot$ and their pair-unstable collapse in the Universe.

I. INTRODUCTION

Gravitational collapse of a carbon-oxygen (CO) core induced by the instability associated with electron-positron pair creation (i.e., pair instability) is a possible fate of a very massive star (VMS) of initial mass $\gtrsim$140 $M_\odot$ [1–4]. Broadly speaking, there are two possible fates for the pair-instability collapse of the VMSs. For the relatively low-mass case, oxygen burning occurs explosively during the collapse, and then the thermal pressure resulting from the thermal energy released by the thermonuclear reaction of oxygen halts the collapse, leading to a pair-instability supernova explosion (PISN). On the other hand, for the high-mass case, the collapse cannot be halted by the nuclear burning, and, hence, the final remnant is a black hole (BH) possibly surrounded by a disk and an outflow [5]. However, PISN and/or BH formation have not been confirmed yet.

In this article, we report a result of our new numerical-relativity simulations for the collapse of a rotating VMS of its initial mass 320 $M_\odot$ to a BH, paying attention to gravitational waves emitted during the BH formation. We show that (i) the gravitational-wave signal is characterized by a ringdown oscillation of the newly formed BH; (ii) for the moderately rapidly rotating cases, the energy emitted by gravitational waves is typically $2 \times 10^{-7} M_{\rm CO} c^2$, where $M_{\rm CO}$ is the mass of the CO core just before the onset of the collapse; (iii) the frequency for the peak amplitude of gravitational waves is 300–600 Hz for $M_{\rm CO} \approx 150~M_\odot$ with the peak amplitude $\sim 10^{-22}$ for a hypothetical distance

to sources $D \sim 50$ Mpc. Such gravitational waves can be a target of third-generation gravitational-wave detectors such as the Einstein Telescope [6].

This paper is organized as follows. In Sec. II, we summarize the setup of our numerical-relativity simulation. In Sec. III, we present the gravitational waveforms to show that these gravitational waves will be a source for third-generation gravitational-wave detectors. Section IV is devoted to a summary and discussion. Throughout this paper, c and G denote the speed of light and gravitational constant, respectively.

II. SETUP

Following Ref. [5], we employ an evolved rotating VMS derived by a stellar evolution code of Refs. [4,7] for preparing the initial conditions for a numerical-relativity simulation. The stellar evolution calculation is performed for a metal-free star of mass 320 $M_\odot$ and of the rigid rotation with the angular velocity of 2.1×10^{-4} s^{-1} at the zero-age main sequence stage. The calculation is continued until the central temperature reaches $\approx 10^{9.2}$ K for which the star is composed of a CO core (mainly of oxygen) and an envelope of helium and hydrogen (see Fig. 2 in Ref. [5]). At this stage, the total mass of the entire star reduces to $\approx$290 $M_\odot$ because of the mass loss during the stellar evolution [8], and the mass of the CO core is $\approx$150 $M_\odot$. The dimensionless spin parameter $cJ_{\rm CO}/(GM_{\rm CO}^2)$ of the CO core is $\approx$1.1.

TABLE I. Quantities for the CO core of VMSs employed in this paper. M_{CO}, the mass. β, the ratio of rotational kinetic energy to gravitational potential energy. J_{CO}, angular momentum and $\chi := cJ_{CO}/(GM_{CO}^2)$. R_{CO}, equatorial radius.

Model	$M_{CO}(M_\odot)$	β	χ	R_{CO} (km)
M01	150	2.7×10^{-5}	0.11	6×10^5
M03	150	2.4×10^{-4}	0.33	6×10^5
M05	150	6.6×10^{-4}	0.55	6×10^5
M07	150	1.3×10^{-3}	0.77	6×10^5
M08	150	1.7×10^{-3}	0.88	6×10^5

In this paper, we explore the collapse of the CO core, reducing its angular velocity uniformly to focus on the collapse of stellar cores for which the dimensionless spin parameter is 0.1–0.9 (see Table I). For these cases, most of the matter in the CO core eventually collapses into a rotating BH. In the following, we pay particular attention to gravitational waves at the formation of the BH, which reflect the early formation process of the BH.

Our method for the solution of Einstein's equation is the same as in Ref. [5]. We employ the original version of the Baumgarte-Shapiro-Shibata-Nakamura formulation with a puncture gauge [9]. The gravitational field equations are solved in the standard fourth-order finite differencing scheme. The axial symmetry is imposed using a fourth-order cartoon method [5,10,11]. Gravitational waves are extracted from the outgoing component of the complex Weyl scalar Ψ_4, which is expanded by a spin-weighted spherical harmonics of weight -2, $_{-2}Y_{lm}(\theta, \varphi)$, with $m = 0$ in axisymmetric spacetime (see, e.g., Ref. [12]). We focus only on the quadrupole mode with $l = 2$ (denoted by Ψ_{20} in the following), because it is the dominant mode (we checked that the amplitude of $l = 3$ and 4 modes is much smaller than the $l = 2$ mode).

The formation of a BH is determined by the presence of an apparent horizon. The mass and dimensionless spin of the BH are determined by measuring the area and circumferential radii of the apparent horizon (e.g., see Ref. [13] for our method).

Following Ref. [5], we use one of the Timmes and Swesty equations of state which includes the contribution from radiation, ions as ideal gas, electrons, positrons, and corrections for Coulomb effects. For electrons and positrons, the relativistic effect, the effects of degeneration, and electron-positron pair creation are taken into account. We also take into account the nuclear burning, photodissociation of iron and helium, and neutrino cooling.

The effect of the neutrino cooling is incorporated in the equation of motion as

$$\nabla_\alpha T^{\alpha\beta} = \rho u^\beta q_{neu} f(\rho), \qquad (2.1)$$

where ∇_α is the covariant derivative with respect to the spacetime metric, $T^{\alpha\beta}$ the energy-momentum tensor, ρ the rest-mass density, u^α the four-velocity of the fluid, q_{neu} the neutrino emission rate of Ref. [14], and $f(\rho)$ a function of ρ, respectively. Neutrinos freely escape from the collapsing core for the case that the density and temperature are not very high. However, for $\rho \gtrsim 10^{11}$ g/cm^3 with the temperature $T \gtrsim 5$ MeV, neutrinos with their cross section $\gtrsim 6 \times 10^{-43}(T/5 \text{ MeV})^2$ cm^2 should be trapped in the collapsing core of radius $\sim 10^7$ cm. To approximately take into account this effect, we introduce a function $f(\rho)$ and set it as $\exp(-\rho/\rho_0)$, where ρ_0 is a constant set to be 10^{11} g/cm^3 at the fiducial runs. In addition, we perform simulations for model M07 with $\rho_0 = 10^{10}$ g/cm^3 and $\rho_0 = 0$ (i.e., $f = 0$) to show that the effect of the neutrino cooling plays a key role for determining the spectrum of gravitational waves.

Numerical simulations are performed in cylindrical coordinates (X, Z), and a nonuniform grid is used for X and Z. Specifically, we employ the following grid spacing (the same profile is chosen for X and Z): For $X_i \leq X_{in}$, $\Delta X = \Delta X_0 = $ const, and for $X_i > X_{in}$, $\Delta X_i = \eta \Delta X_{i-1}$. ΔX_0 is the grid spacing in an inner region, and $\Delta X_i := X_{i+1} - X_i$ with X_i the location of the ith grid. η determines the nonuniform degree of the grid spacing for which we always choose 1.014. As in Ref. [5], for the early stage of the collapse, we employ large values of ΔX_0 and X_{in} for which we assign the same values as before [5], and then we perform a regridding for a better-resolved simulation. For this later phase, we employ a grid resolution better than in our previous study [5] as $\Delta X_0 = 0.0048$–$0.0096 GM_{CO}/c^2(\approx 1.1$–$2.2)$ km. By varying ΔX_0 for such a range, we confirmed that the convergence of the gravitational waveform is well achieved.

III. NUMERICAL RESULTS

A. Black hole formation processes

For all the models considered in this paper, a BH is formed in the CO core collapse. However, the formation and evolution processes of the BH depend strongly on the effect of the nuclear reaction and neutrino cooling.

The left panel in Fig. 1 shows the evolution of the mass and dimensionless spin for M07 models with no nuclear reaction and $f(\rho) = 0$ (no neutrino cooling) and with the nuclear reaction and various values of ρ_0, 0, 10^{10}, and 10^{11} g/cm^3. This shows that, for no nuclear reaction, a substantial fraction of the CO core collapses into a BH in the first ~ 50 ms. By contrast, in the presence of the nuclear reaction (i.e., in the more realistic case), the initial mass of the BH is much smaller than the total mass of the CO core. The reason for this is that the photodissociation of iron and helium significantly reduces the thermal pressure in the central region of the collapsing core, and, as a result, the collapse of the central region is significantly accelerated, leading to a runaway collapse.
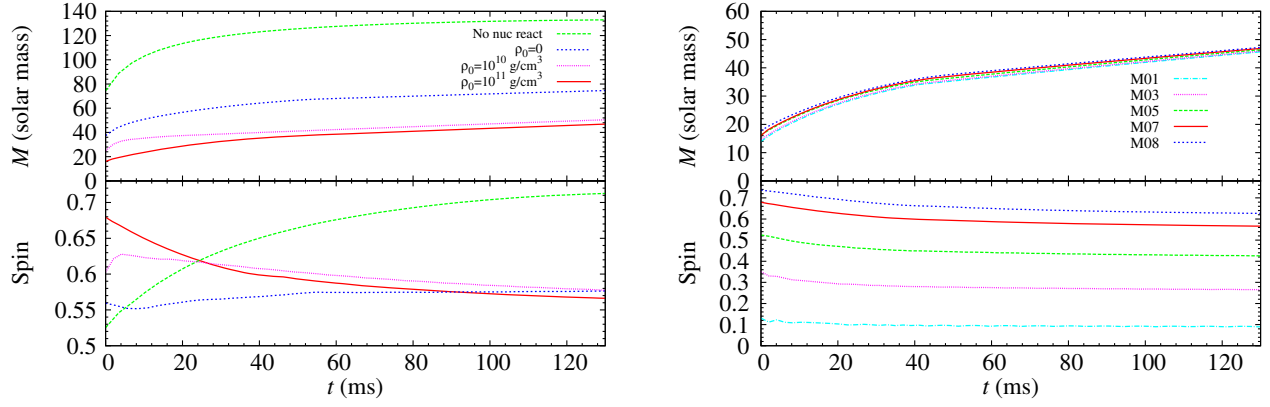
FIG. 1.   Left: Evolution of mass and dimensionless spin of a BH formed after the collapse of VMSs for M07 models. The dashed green, dotted blue, short-dotted magenta, and solid red curves show the results for no nuclear reaction and for the presence of the nuclear reaction with $\rho_0 = 0$, 10^{10}, and 10^{11} g/cm^3, respectively. We note that, for the models in which the neutrino cooling is more efficient (for larger values of ρ_0), the initial BH mass is smaller. Right: The same as the left panel but for models M01, M03, M05, M07, and M08 in the presence of the nuclear reaction and the neutrino cooling with $\rho_0 = 10^{11}$ g/cm^3.

In addition to the nuclear reaction, the neutrino cooling plays an important role in determining the initial BH mass M_i. For no neutrino cooling [i.e., $f(\rho) = 0$ or $\rho_0 = 0$], $M_i \sim 40\ M_\odot$. On the other hand, if we take into account the neutrino cooling ($\rho_0 = 10^{10}$ and 10^{11} g/cm^3), M_i is smaller as $\sim$20–30 $M_\odot$; i.e., for the larger value of ρ_0, M_i is smaller. The reason for this is that, by the neutrino cooling, the collapse is further accelerated in the central region, leading to a smaller initial BH mass.

By contrast to the BH mass, the initial dimensionless spin is in a fairly narrow range between 0.53 and 0.68, and, thus, it does not depend strongly on the effects of nuclear reaction and neutrino cooling for the M07 models. This property simply reflects the initial angular momentum distribution of the CO core at the onset of the collapse.

The right panel in Fig. 1 shows the evolution of the mass and dimensionless spin for models M01, M03, M05, M07, and M08 with the nuclear reaction and with the neutrino cooling for $\rho_0 = 10^{11}$ g/cm^3. This illustrates that the

evolution of the BH mass depends only weakly on the total angular momentum of the collapsing star. On the other hand, the BH spin naturally reflects the angular momentum distribution of the CO cores.

B. Gravitational waves

Figure 2 displays gravitational waveforms (Ψ_{20}) as a function of retarded time. Here, the time at which the maximum amplitude is reached is chosen as the origin of the time. We note that the $l = 2$, $m = 0$ mode is proportional to $\sin^2 \theta$, where θ is the angle from the rotation axis. Thus, the amplitude becomes maximum for an observer located along the equatorial plane, and it vanishes if the observer is located along the rotation axis. Figure 2 plots the waveforms for $\theta = \pi/2$.

Figure 2 shows that gravitational waves are composed of a short precursor and ringdown oscillation associated with the formed BH for all the models considered in this paper.
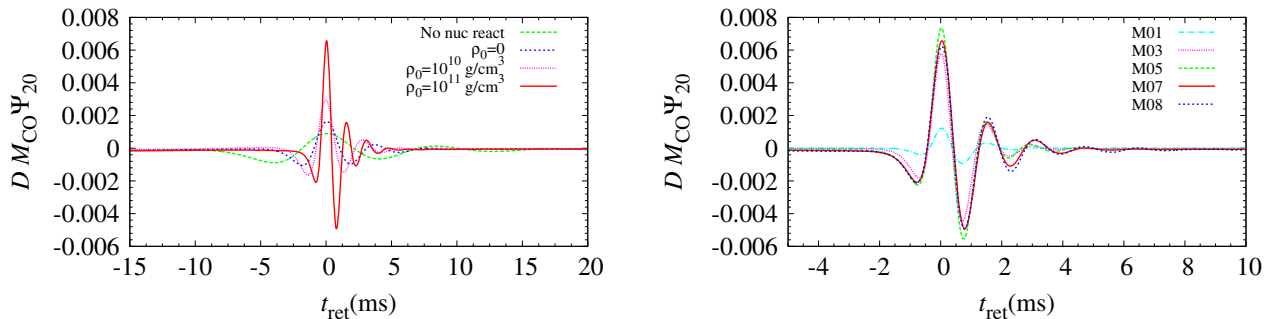
FIG. 2.   Left: Gravitational waveforms ($l = 2$ axisymmetric mode of Ψ_4) as a function of retarded time for M07 models with no nuclear reaction (green dashed curve) and with the nuclear reaction and neutrino cooling ($\rho_0 = 10^{11}$ g/cm^3, solid red curve; $\rho_0 = 10^{10}$ g/cm^3, short-dotted magenta curve; and $\rho_0 = 0$, dotted blue curve). Right: The same as the left panel but for models M01, M03, M05, M07, and M08 in the presence of the nuclear reaction and the neutrino cooling with $\rho_0 = 10^{11}$ g/cm^3. For these figures, the time at which the maximum amplitude is reached is chosen as the origin of the time to align the waveforms.
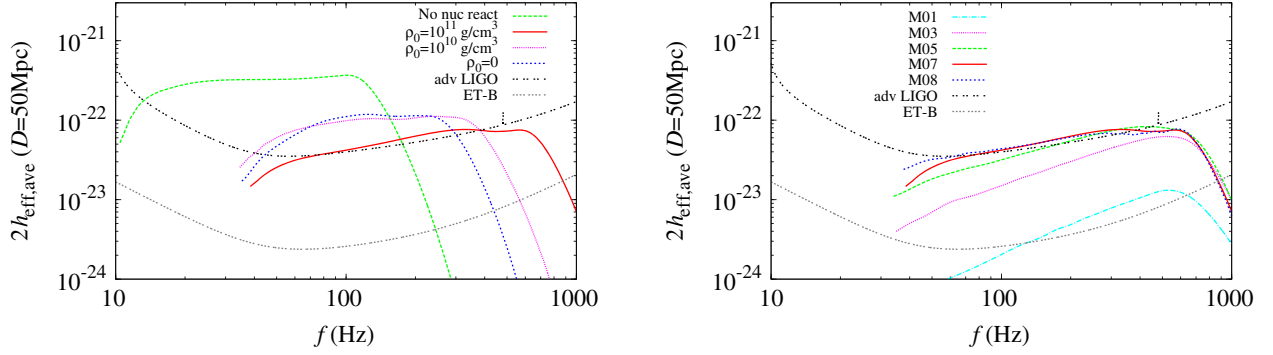
FIG. 3.   Left: Fourier spectrum of gravitational waves for a hypothetical distance to the source $D = 50$ Mpc for M07 models. Here, we plot $2h_{\text{eff,ave}} = 2h_{\text{eff}} \times 2/3$. Each line type denotes the same model as in the left panel in Fig. 2. The black dot-dot and gray dot-dot-dot curves show the design sensitivities of the advanced LIGO (the "zero detuning high power" configuration [19]) and Einstein Telescope of type B [20]. Right: The same as the left panel but for models M01, M03, M05, M07, and M08. Each line type denotes the same model as in the right panel in Fig. 2.

The period of the ringdown oscillation, λ, is varied for each model. We note that, for the $l = 2$, $m = 0$ mode, λ should be $\approx 16GM_{\text{BH}}/c^3 \approx 1.6(M_{\text{BH}}/20\, M_\odot)$ ms, where M_{BH} is the mass of the BH, according to the linear-perturbation analysis for the BH quasinormal modes [15] with dimensionless spin, $\chi_{\text{BH}} = 0$–0.8. For all the models with the nuclear reaction, λ agrees approximately with that predicted by the BH perturbation theory if we take the initial mass of the BH as M_{BH}. Thus, the gravitational waveforms reflect the early formation process of the BH. For the model with no nuclear reaction (dashed green curve in the left panel in Fig. 2), $\lambda \sim 16 \times (100GM_\odot/c^3) \sim 8$ ms, reflecting the fact that a substantial fraction of the CO core matter simultaneously collapses into the BH.

The right panel in Fig. 2 shows that the gravitational waveforms depend weakly on the BH spin for $\chi \gtrsim 0.5$. The main reason for this is that the evolution process of the BH mass depends only weakly on the spin. For $\chi \lesssim 0.3$, the maximum amplitude decreases steeply with the decrease of χ. This reflects the fact that, for such small values of χ, the degree of axial symmetry decreases with χ. For higher BH spins, the damping time for the ringdown oscillation is longer. This also agrees with the prediction by the BH perturbation theory [15]. For $\chi \gtrsim 0.5$, the peak amplitude is slightly higher for the lower spin. This reflects the fact that, for the higher spin, the collapse is decelerated by a stronger centrifugal force, and the gravitational-wave emission is slightly suppressed.

The total energy of gravitational waves emitted is $\Delta E \approx 7 \times 10^{-7} M_{\text{CO}} c^2$ for the model with no nuclear reaction and $\approx 2 \times 10^{-7} M_{\text{CO}} c^2$ for the models with the nuclear reaction and $\chi \gtrsim 0.5$. Thus, the emissivity is suppressed in the presence of the nuclear reaction (specifically, photodissociation). The emissivity is much smaller than those in binary BH mergers in which $\sim 10\%$ of the total mass energy can be radiated (e.g., Ref. [16]). The emissivity for no nuclear reaction is as large as that for the collapse of

supermassive stars to a BH [17]. For $\chi \lesssim 0.5$, ΔE steeply decreases with χ: $\Delta E/(M_{\text{CO}} c^2) \approx 4 \times 10^{-9}$ and 1×10^{-7} for M01 and M03, respectively.

Figure 3 shows a spectrum (an effective amplitude) of gravitational waves for $D = 50$ Mpc for M07 models. Here, the Fourier spectrum $h(f)$ is first derived from [12]

$$h(f) = -_{-2}Y_{20}\int_{-t_i}^{t_f} dt\,\frac{2\Psi_{20}(t)}{(2\pi f)^2}\exp(-2\pi i f t), \qquad (3.1)$$

where $t_i = t_f \approx 10$–30 ms for the choice of time in which the maximum of Ψ_{20} is reached at $t = 0$. Here, t_i and t_f are varied depending on the characteristic wavelength of gravitational waves. Since $_{-2}Y_{20}$ is proportional to $\sin^2\theta$, the average of $h(f)$ with respect to θ is $h_{\text{ave}}(f) = 2h(f)_{\theta=\pi/2}/3$. Then, we define the effective amplitude by $h_{\text{eff,ave}} := f|h_{\text{ave}}(f)|$ [18]. In Fig. 3, we, in addition, multiply by 2, because the signal-to-noise ratio (SNR) for a spectrum of gravitational waves, $g(f)$, is written as

$$\text{SNR} = \int_0^\infty df\,\frac{(2|g(f)|)^2}{S_n(f)}, \qquad (3.2)$$

where $S_n(f)$ is the one-sided noise spectrum density of a gravitational-wave detector [i.e., for each frequency f, $2|fh(f)|/\sqrt{S_n(f)f}$ approximately denotes the SNR]. The black dot-dot and gray dot-dot-dot curves show the design sensitivities of advanced LIGO (the zero detuning high power configuration [19]) and the Einstein Telescope of type B [20]. Here, we plot a dimensionless quantity $(S_n f)^{1/2}$. We note that a low-frequency part of $h(f)$ depends on the choice of t_i and t_f, and, hence, we do not plot the unreliable part of $h_{\text{eff,ave}}$ in Fig. 3.

Figure 3 shows that the peak amplitude of $h_{\text{eff,ave}}$ is proportional approximately to the initial mass of the formed BH. On the other hand, the highest frequency

for the peak amplitude is inversely proportional to the BH mass. Broadly speaking, for the initial BH mass M_i, the maximum value of $2h_{\mathrm{eff,ave}}$ is written as $\sim 10^{-22}(M_i/30\,M_\odot)$, and the corresponding highest frequency is $\sim 400(M_i/30\,M_\odot)^{-1}$ Hz. As indicated from the right panel in Fig. 2, these values depend very weakly on the angular momentum of the CO cores for $\chi \gtrsim 0.5$.

For the curves shown in Fig. 3, the SNR for the most optimistic alignment of a detector with respect to the direction of the source (see [18] for a remark) is calculated for $D = 50$ Mpc. For the sensitivity of advanced LIGO, it becomes ≈ 11 for the model with no nuclear reaction and no neutrino cooling, ≈ 3.1 for the models with the nuclear reaction and $\rho_0 = 0$ and 10^{10} g/cm^3, and ≈ 1.7 with the nuclear reaction and $\rho_0 = 10^{11}$ g/cm^3. For the sensitivity of the Einstein Telescope of type B, on the other hand, each value is enhanced as 164, 47, 46, and 24, respectively. Obviously, for a higher value of M_i, the SNR is higher. However, the most realistic models are those with the nuclear reaction and $\rho_0 = 10^{11}$ g/cm^3 (for which SNR = 1.7). This implies that, for the second-generation detectors (advanced LIGO, advanced VIRGO, and KAGRA), it would be difficult to detect gravitational waves emitted by the collapse of a VMS of initial mass $\sim 300\,M_\odot$ unless the collapse occurs for $D \lesssim 10$ Mpc. However, with the third-generation detectors such as the Einstein Telescope, these gravitational waves could be detected with SNR $\gtrsim 10$ for events with $D \lesssim 100$ Mpc.

The right panel in Fig. 3 shows the spectrum for models M01, M03, M05, M07, and M08. This shows that, for $\chi \gtrsim 0.5$, the peak amplitude depends weakly on the value of χ, but, for the small values of χ, it decreases steeply, and, in addition, the amplitude becomes steeply small with the decrease of f. Thus, to get a high SNR, a moderately large value of $\chi \gtrsim 0.5$ is necessary.

IV. SUMMARY AND DISCUSSION

By new numerical-relativity simulations, we derived gravitational waveforms from a rotating VMS core collapsing

to a BH and found that they are characterized by a ringdown oscillation of the formed BH in its early formation phase. For a plausible setting of the nuclear reaction and neutrino cooling, the initial BH mass is $\approx 20\,M_\odot$ for $M_{\mathrm{CO}} \approx 150\,M_\odot$. For the moderately rapidly rotating case, gravitational waves have a broad peak in the spectrum for $f \approx 300\text{--}600$ Hz with $h_{\mathrm{eff,ave}} \sim 10^{-22}$ for $D = 50$ Mpc, for which the SNR for the designed sensitivities of advanced LIGO and the Einstein Telescope of type B would be $\lesssim 2$ and 20, respectively. Thus, it would be difficult to detect such gravitational waves by the second-generation detectors, but they will be one of the targets for the third-generation detectors.

We should keep in mind that, for very massive CO cores ($M_{\mathrm{CO}} \gg 150\,M_\odot$), the initial BH mass would be much higher, say, $100\,M_\odot$. For such a case, the peak effective amplitude of gravitational waves would be $\sim 4 \times 10^{-22}$, and the corresponding characteristic frequency would be ~ 100 Hz (see Fig. 3). For these gravitational waves, the SNR can be ~ 10 for $D = 100$ Mpc for the designed sensitivity of advanced LIGO. Thus, for such a VMS collapse, gravitational waves would have an SNR high enough for detection by the second-generation detectors.

As we illustrated in Ref. [5], electromagnetic signals could be emitted after the BH formation in the collapse of rotating VMSs. Detection of gravitational waves will be used for constraining the sky location for the search of such electromagnetic signals, which could give important information on the BH formation and subsequent evolution of the system.

[1] C. L. Fryer, S. E. Woosley, and A. Heger, Astrophys. J. **550**, 372 (2001).

[2] A. Heger and S. E. Woosley, Astrophys. J. **567**, 532 (2002).

[3] H. Umeda and K. Nomoto, Astrophys. J. **565**, 385 (2002).

[4] K. Takahashi, T. Yoshida, H. Umeda, K. Sumiyoshi, and S. Yamada, Mon. Not. R. Astron. Soc. **456**, 1320 (2016).

[5] H. Uchida, M. Shibata, K. Takahashi, and T. Yoshida, Astrophys. J. **870**, 15 (2019).

[6] S. Hild et al., Classical Quantum Gravity **28**, 094013 (2011).

[7] K. Takahashi, T. Yoshida, and H. Umeda, Astrophys. J. **857**, 111 (2018).

[8] S. C. Yoon, S. E. Woosley, and N. Langer, Astrophys. J. **725**, 940 (2010); S. C. Yoon, A. Dierks, and N. Langer, Astron. Astrophys. **542**, A113 (2012).

[9] M. Shibata and T. Nakamura, Phys. Rev. D **52**, 5428 (1995); T. W. Baumgarte and S. L. Shapiro, Phys. Rev. D **59**, 024007 (1998); M. Campanelli, C. O. Lousto, P. Marronetti,

and Y. Zlochower, Phys. Rev. Lett. **96,** 111101 (2006); J. G. Baker, J. Centrella, D.-I. Choi, M. Koppitz, and J. v. Meter, Phys. Rev. Lett. **96,** 111102 (2006).

[10] M. Alcubierre, B. Brügmann, D. Holz, R. Takahashi, S. Brandt, E. Seidel, and J. Thornburg, Int. J. Mod. Phys. D **10,** 273 (2001).

[11] M. Shibata, Prog. Theor. Phys. **104,** 325 (2000); Phys. Rev. D **67,** 024033 (2003).

[12] T. Yamamoto, M. Shibata, and K. Taniguchi, Phys. Rev. D **78,** 064054 (2008).

[13] K. Kyutoku, M. Shibata, and K. Taniguchi, Phys. Rev. D **82,** 044049 (2010).

[14] N. Itoh, H. Hayashi, A. Nishikawa, and Y. Kohyama, Astrophys. J. Suppl. Ser. **102,** 411 (1996).

[15] E. Berti, V. Cardoso, and A. O. Starinets, Classical Quantum Gravity **26,** 163001 (2009).

[16] G. Lovelace, M. Boyle, M. A. Scheel, and B. Szilágyi, Classical Quantum Gravity **29,** 045003 (2012); D. A. Hemberger, G. Lovelace, T. J. Loredo, L. E. Kidder, M. A. Scheel, B. Szilágyi, N. W. Taylor, and S. A. Teukolsky, Phys. Rev. D **88,** 064014 (2013).

[17] M. Shibata, Y. Sekiguchi, H. Uchida, and H. Umeda, Phys. Rev. D **94,** 021501(R) (2016).

[18] If we further take into account the antenna pattern of the gravitational-wave detectors with respect to the injection direction of gravitational waves, the root-mean square of the actual amplitude which the detectors measure would be by a factor of $1/\sqrt{5}$ smaller.

[19] https://dcc.ligo.org/cgi-bin/DocDB/.

[20] http://www.et-gw.eu.